J. Appl. Comput. Mech., 5(5) (2019) 935-950
DOI: 10.22055/JACM.2019.28296.1474

ISSN: 2383-4536
jacm.scu.ac.ir

M&MoCS

Shahid Chamran University of Ahvaz

Journal of Applied and Computational Mechanics

Research Paper

Analysis of the Coupled Nonlinear Vibration of a Two-Mass System

Akuro Big-Alabo[1], Chinwuba Victor Ossia[2]

[1] Department of Mechanical Engineering, Faculty of Engineering, University of Port Harcourt
Port Harcourt, Nigeria, akuro.big-alabo@uniport.edu.ng

[2] Department of Mechanical Engineering, Faculty of Engineering, University of Port Harcourt
Port Harcourt, Nigeria, chinwuba.ossia@uniport.edu.ng

Received January 19 2019; Revised April 04 2019; Accepted for publication April 15 2019.
Corresponding author: Akuro Big-Alabo, akuro.big-alabo@uniport.edu.ng

Abstract. This paper presents a fixed-end two-mass system (TMS) with end constraints that permits uncoupled solutions for different masses. The coupled nonlinear models for the present fixed-end TMS were solved using the continuous piecewise linearization method (CPLM) and detailed investigation on the effect of mass-ratio on the TMS response was conducted. The investigations showed that increased mass-ratio leads to decreased oscillation frequency and an asymptotic response was obtained at very large mass-ratios. Theoretical solutions to determine the asymptotic response were derived. Also, it was observed that distinct responses can be obtained for the same mass-ratio depending on the mass combination in the TMS. The present fixed-end TMS and the analyses presented give a broader understanding of fixed-end TMS.

Keywords: Continuous piecewise linearization method, Two-mass system, Cubic Duffing oscillator, Coupled nonlinear vibration.

1. Introduction

The coupled nonlinear vibrations of a TMS describe the dynamic response of important engineering systems. The vibrations of a milling machine, marine engine propeller system, micro-electro-mechanical system (MEMS) and double beam structure are examples of practical two-mass systems that have coupling springs and can exhibit coupled nonlinear vibration. The problem of coupled nonlinear vibrations of a two-mass system has been investigated in several studies [1-9]. The basic physical model involves two masses connected by a coupling nonlinear spring moving in two degrees-of-freedom (DOF) and the resulting mathematical models consist of two coupled nonlinear ordinary differential equations (ODEs). By means of intermediate transformation variables the coupled nonlinear ODEs can be reduced to a single nonlinear ODE that describes the relative motion of the masses [3, 4]. This way, the solution for the vibration response of the masses is determined from the solution of the relative motion. Alternatively, intermediate variables can be introduced to transform the coupled nonlinear ODEs into a set of two single-DOF ODEs; one linear and the other nonlinear [1, 2]. The single-DOF nonlinear ODE represents the relative motion of the masses while the single-DOF linear ODE represents the cumulative motion of the masses. Consequently, the vibrations of the masses are determined by solving the linear and nonlinear ODEs simultaneously.

A TMS can be classified based on the constraint at the end of the coupled masses as (a) free-end TMS (see Fig. 1) and (b) fixed-end TMS (see Fig. 2). The free-end TMS has no constraint at the end of the masses and can be treated as a special case of the fixed-end TMS that has constraints at the end of the masses. Hence, the solution for a free-end TMS can be derived from the solution of a fixed-end TMS.

The conventional fixed-end TMS that appears in the literature [1, 3-6] is based on identical masses. This is because the end constraints can only permit uncoupled solutions when the masses are identical. If the masses were different then the response of the conventional fixed-end TMS cannot be uncoupled and analytical solutions become intractable. This may explain why studies to investigate the effect of mass-ratio on the vibration response of the fixed-end TMS do not appear in the literature.

Published online: June 10 2019

Such studies are important because it can be used for design purposes. To overcome this shortcoming, this paper presents a fixed-end TMS with end constraints that permit uncoupled solutions when the masses are different. The dynamic models derived are in the form of coupled nonlinear ODEs and were solved using an approximate analytic algorithm called "continuous piecewise linearization method" [10]. Although several analytical solutions have been published for the fixed-end TMS with identical masses [1, 3-6], the CPLM algorithm was used in the present study because of its simplicity, accuracy and ability to obtain uncoupled solutions easily. As a main objective, investigations were conducted on the effect of mass ratio on the vibration response of the fixed-end TMS. The results obtained reveal interesting asymptotic behavior of the TMS.

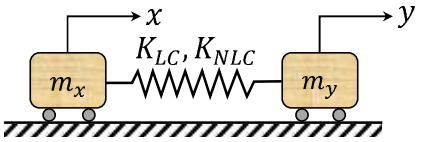

Fig. 1. Schematic of two-mass system with free ends.

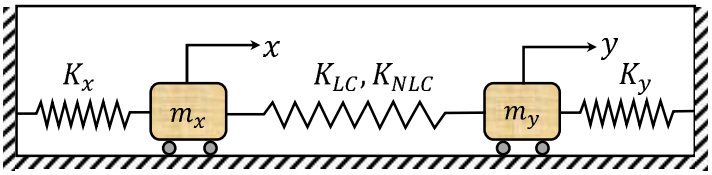

Fig. 2. Schematic of two-mass system with fixed ends.

2. Nonlinear Models for New Fixed-End Two-Mass System

The fixed-end TMS consists of two rigid masses connected to each other by a coupling spring having linear and cubic nonlinear stiffness characteristics. The end of each mass is constrained by a linear spring connection to a frame as shown in Fig. 2. In the conventional fixed-end TMS, $K_x = K_y = K_L$ where K_L is a linear stiffness constant. This end constraint condition can only permit uncoupled solutions when $m_x = m_y = m$. In the present study, the fixed-end TMS that was investigated is such that the linear springs used to connect the masses to the frame have different stiffnesses with a ratio that is equal to the ratio of the corresponding masses i.e. $K_y / K_x = m_y / m_x$. This new end constraint allows for uncoupled solutions when $m_x \neq m_y$ and at the same time permits analysis of the effect of mass ratio on the vibration response of the system. The modification in the fixed-end TMS proposed here to incorporate different masses broadens the scope of applicability of the system. The equations governing the vibrations of the masses in Fig. 2 are readily derived as [3-6]:

$$m_x x'' + K_x x + K_{LC}(x-y) + K_{NLC}(x-y)^3 = 0 \tag{1}$$

$$m_y y'' + K_y y + K_{LC}(y-x) + K_{NLC}(y-x)^3 = 0 \tag{2}$$

The initial conditions for the above 2-DOF system are: $x(0) = X_0$; $y(0) = Y_0$; $x'(0) = 0$ and $y'(0) = 0$. Applying the end constraint that $K_y / K_x = r_m$ where $K_x = K_L$ gives:

$$m_x x'' + K_L x + K_{LC}(x-y) + K_{NLC}(x-y)^3 = 0 \tag{3}$$

$$m_y y'' + r_m K_L y + K_{LC}(y-x) + K_{NLC}(y-x)^3 = 0 \tag{4}$$

where $r_m = m_y / m_x$. It is obvious that $r_m = 1$ gives the conventional fixed-end TMS, which is a special case of the present fixed-end TMS. Let $z = y - x$ be an intermediate transformation variable. Therefore, Eqs. (3) and (4) become

$$m_x x'' + K_L x - K_{LC} z - K_{NLC} z^3 = 0 \tag{5}$$

$$m_y y'' + r_m K_L y + K_{LC} z + K_{NLC} z^3 = 0 \tag{6}$$

Since $y = x + z$ then Eq. (6) can be written as:

$$m_y (x'' + z'') + r_m K_L (x + z) + K_{LC} z + K_{NLC} z^3 = 0 \tag{7}$$

From Eq. (5),

$$x'' = \frac{K_{LC}}{m_x} z + \frac{K_{NLC}}{m_x} z^3 - \frac{K_L}{m_x} x \tag{8}$$

Substituting Eq. (8) into Eq. (7) and after simplification, the nonlinear ODE for the relative motion becomes:

$$z'' + \alpha z + \beta z^3 = 0 \tag{9}$$

where $\alpha = K_L / m_x + K_{LC} / m$; $\beta = K_{NLC} / m$; $m = \left(1/m_x + 1/m_y\right)^{-1}$ is the effective mass and the initial conditions are: $z(0) = Y_0 - X_0 = A$ and $z'(0) = 0$. Equation (9) can be solved using the CPLM algorithm. The solution of the *z*-motion can be used to get the solution for the *x*-motion from Eq. (8) and the *y*-motion from the intermediate variable definition.

3. Analytical Algorithm for Solution of Two-Mass System

The CPLM is an iterative analytical algorithm that can be used to obtain periodic solutions of nonlinear conservative Duffing-type oscillators [10]. It was formulated based on continuous piecewise linearization of the nonlinear restoring force with respect to displacement. The piecewise discretization and linearization technique applied by the CPLM was first used in the formulation of another analytical algorithm called force-indentation linearization method (FILM) that was designed to solve nonlinear models of half-space impact [11]. Subsequently, the FILM has been applied in a more general form to obtain solutions for asymptotic impact problems characterized by significant localized indentations [12]. In recent studies [13, 14], the FILM was used to derive uncoupled solutions for the elastoplastic impact of two spheres thus leading to the development of a new spherical modelling approach called equivalent impact system approach (EISA) [14]. However, the FILM cannot be used to obtain periodic solutions of nonlinear oscillating systems because it is restricted to non-oscillating forces and displacements. The CPLM removes these restrictions and can be viewed as a modification of the FILM to enable periodic solutions of nonlinear oscillating systems. Therefore the CPLM retains all the advantages [12] of the FILM. In this section, the CPLM was applied to obtain solutions for the relative motion (*z*-motion) and coordinate motions (*x*- and *y*-motions).

3.1. CPLM Solution for Two-Mass System with Fixed Ends

3.1.1. Solution of Relative Motion (*z*-motion) for the Case of Fixed Ends

From Eq. (9) we can write:

$$z'' + F(z) = 0 \tag{10}$$

where $F(z) = \alpha z + \beta z^3$ is the nonlinear restoring force. According to the CPLM [10], the linearized restoring force for each *n* discretization bounded by points *r* and *s* can be written as:

$$F(z) = K_{rs}(z - z_r) + F(z_r) \tag{11}$$

where $K_{rs} = \left|\left[F(z_s) - F(z_r)\right] / (z_s - z_r)\right|$ is the linearized stiffness for each discretization, $r = 0,1,2,3,\ldots, n-1$ is the start point of each discretization, $s = r + 1$ is the end point of each discretization and *n* is the number of discretization used. Substituting Eq. (11) in Eq. (10) gives the linearized equation of motion for each discretization as:

$$z'' + \omega_{rs}^2 z = \omega_{rs}^2 z_r - F(z_r) \tag{12}$$

where $\omega_{rs} = \sqrt{K_{rs}}$. The solution to Eq. (12) is given as:

$$z = R_{rs} \sin\left(\omega_{rs} t + \varphi_{rs}\right) + C_{rs} \tag{13a}$$

From Eq. (13a), we get:

$$z' = \omega_{rs} R_{rs} \cos\left(\omega_{rs} t + \varphi_{rs}\right) \tag{13b}$$

The constants in Eq. (13) are calculated as: $C_{rs} = z_r - F(z_r) / K_{rs}$ and $R_{rs} = \sqrt{\left(z_r - C_{rs}\right)^2 + \left(z_r' / \omega_{rs}\right)^2}$. The expression for R_{rs} shows that it depends on the initial conditions, which are determined together with other parameters based on the stage of the oscillation. For the oscillation stage where the velocity is negative (see path *b* – *c* – *d* in Fig. 3) the initial conditions for each discretization are $z_r = z_r(0) = A - r\Delta z$ and $z_r' = z_r'(0) = -\sqrt{\left|2\int_A^{z_r} -F(z)\,dz\right|}$; where $\Delta z = A / n$ and the other parameters are calculated as:

$$\varphi_{rs} = \begin{cases} 0.5\pi & z_r' = 0 \\ \pi + \tan^{-1}\left[\omega_{rs}\left(z_r - C_{rs}\right) / z_r'\right] & z_r' < 0 \end{cases}$$

$$\Delta t = \begin{cases} \left(0.5\pi - \varphi_{rs}\right)/\omega_{rs} & \left(z_s - C_{rs}\right) \geq R_{rs} \\ \left(0.5\pi + \cos^{-1}\left[\left(z_s - C_{rs}\right) / R_{rs}\right] - \varphi_{rs}\right)/\omega_{rs} & \left(z_s - C_{rs}\right) < R_{rs} \end{cases}$$

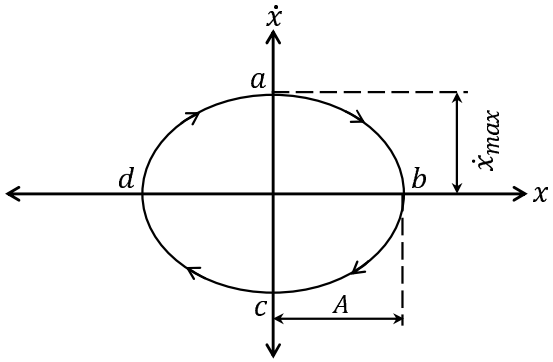

Fig. 3. Typical phase diagram for Duffing-type oscillations.

If the oscillation stage is such that the velocity is positive (see path $d-a-b$ in Fig. 3) then the initial conditions for each discretization are $z_r = z_r(0) = -A + r\Delta z$ and $z_r' = z_r'(0) = \sqrt{\left|2\int_A^{z_r} -F(z)dz\right|}$, whereas the other parameters are calculated as:

$$\varphi_{rs} = \begin{cases} -0.5\pi & z_r' = 0 \\ \tan^{-1}\left[\omega_{rs}\left(z_r - C_{rs}\right)/z_r'\right] & z_r' > 0 \end{cases}$$

$$\Delta t = \begin{cases} \left(0.5\pi - \varphi_{rs}\right)/\omega_{rs} & \left(z_s - C_{rs}\right) \geq R_{rs} \\ \left(0.5\pi - \cos^{-1}\left[\left(z_s - C_{rs}\right)/R_{rs}\right] - \varphi_{rs}\right)/\omega_{rs} & \left(z_s - C_{rs}\right) < R_{rs} \end{cases}$$

Lastly, the end conditions z_s and z_s' are calculated by replacing r with s in the formulae for initial conditions and the time at the end of each discretization is calculated as $t_s = t_r + \Delta t$. With the exception of the first discretization, the initial conditions for the i^{th} discretization are the same as the end conditions for the $(i-1)^{\text{th}}$ discretization; i.e. $z_r^i = z_s^{i-1}$ and $\left(z_r'\right)^i = \left(z_s'\right)^{i-1}$. The solution for each discretization (Eq. (13)) can be used to plot the oscillation histories within the time interval $t_r \leq t \leq t_s$.

3.1.2. Solution of *x*-motion for the Case of Fixed Ends

In order to derive the solution for the x-motion of fixed-end TMS, we start with Eq. (8) and rewrite as shown below:

$$x'' + \frac{K_L}{m_x}x = \frac{K_{LC}}{m_x}z + \frac{K_{NLC}}{m_x}z^3 \tag{14}$$

By comparing $F(z) = \alpha z + \beta z^3$ with the right hand side of Eq. (14), the following relation can be obtained:

$$\frac{K_{LC}}{m_x}z + \frac{K_{NLC}}{m_x}z^3 = \frac{m}{m_x}\left[F(z) - \frac{K_L}{m_x}z\right] \tag{15}$$

Substituting the above relation in Eq. (14) gives:

$$x'' + \frac{K_L}{m_x}x = \frac{m}{m_x}\left[F(z) - \frac{K_L}{m_x}z\right] \tag{16}$$

From Eqs. (11) and (13a) the linearized restoring force for each discretization can be expressed as an explicit function of time as shown:

$$F(z) = K_{rs}R_{rs}\sin\left(\omega_{rs}t + \varphi_{rs}\right) \tag{17}$$

Therefore, using Eqs. (13a) and (17) in Eq. (16) results in a non-homogeneous linear ODE for the x-motion as shown in Eq. (18).

$$x'' + \omega_x^2 x = A_{rs}\sin\left(\omega_{rs}t + \varphi_{rs}\right) + H_{rs} \tag{18}$$

where $A_{rs} = \left(m/m_x\right)\left(\omega_{rs}^2 - \omega_x^2\right)R_{rs}$; $H_{rs} = -\left(m/m_x\right)\omega_x^2 C_{rs}$; and $\omega_x = \sqrt{K_L/m_x}$. The complete solution to Eq. (18) is:

$$x = x_H + x_P = A_1\sin\left(\omega_x t\right) + A_2\cos\left(\omega_x t\right) - \left(m/m_x\right)R_{rs}\sin\left(\omega_{rs}t + \varphi_{rs}\right) + H_{rs}/\omega_x^2 \tag{19}$$

where $A_1 = \left(x_r - x_{Pr}\right)\sin\left(\omega_x t_r\right) + \left[\left(x_r' - x_{Pr}'\right)/\omega_x\right]\cos\left(\omega_x t_r\right)$ and $A_2 = \left(x_r - x_{Pr}\right)\cos\left(\omega_x t_r\right) - \left[\left(x_r' - x_{Pr}'\right)/\omega_x\right]\sin\left(\omega_x t_r\right)$. Applying

Eq. (13a) in Eq. (19) and noting that $H_{rs} = -(m/m_x)\omega_x^2 C_{rs}$, the displacement of the *x*-motion is simplified as shown:

$$x = A_1 \sin(\omega_x t) + A_2 \cos(\omega_x t) - \left(\frac{m}{m_x}\right) z \tag{20}$$

where $x_P = -(m/m_x)z$. In evaluating the expressions for A_1 and A_2 the value of the particular solution at initial condition is required and can be calculated as $x_{Pr} = -(m/m_x)z_r$ and $x'_{Pr} = -(m/m_x)z'_r$. Differentiating Eq. (20) gives the velocity of the *x*-motion as:

$$x' = \omega_x \left[A_1 \cos(\omega_x t) - A_2 \sin(\omega_x t)\right] - \left(\frac{m}{m_x}\right) z' \tag{21}$$

3.1.3. Solution of *y*-motion for the Case of Fixed Ends

Based on the intermediate variable definition, the displacement and velocity of the *y*-motion are respectively given as:

$$y = A_1 \sin(\omega_x t) + A_2 \cos(\omega_x t) + \left(1 - \frac{m}{m_x}\right) z \tag{22}$$

$$y' = \omega_x \left[A_1 \cos(\omega_x t) - A_2 \sin(\omega_x t)\right] + \left(1 - \frac{m}{m_x}\right) z' \tag{23}$$

From the above solutions derived for the fixed-end TMS it is obvious that the CPLM solution is simple and easy to implement. Interestingly, the CPLM solution for the vibrations of the masses remains the same even if a more complex nonlinearity, e.g. quintic nonlinearity, is considered. The only change involved is the expression for $F(z)$ which will then be equal to the new restoring force. In contrast, the solutions based on other approximate methods become more complicated as the nonlinearity becomes more complex and in some cases the solutions may be impractical (e.g. Lai and Lim [3]).

The solutions of the *x*- and *y*-motions derived for the TMS with fixed ends (see Eqs. (20 – 23)) are independent of the discretization process of the CPLM because they do not contain any constants that depend on the discretization i.e. constants having a subscript of *rs*. Therefore, the solutions derived are exact closed-form solutions of the *x*- and *y*-motions expressed in terms of the relative motion. This means that once the solution of the relative motion has been derived by any method for solving single-DOF nonlinear ODE, the closed-form solutions can be used to compute the vibration response of the masses.

3.1.4. Solution of *x*- and *y*-motions for the Case of Free Ends

The ends of the TMS are free when $K_L = 0$. Hence, starting from Eq. (14) and working through the algebra, the solution of the *x*-motion for the free-end TMS was derived as:

$$x = x(t_r) - \frac{m}{m_x}\left[z - z(t_r)\right] + \left[\frac{m}{m_x} z'(t_r) + x'(t_r)\right](t - t_r) \tag{24}$$

$$x' = x'(t_r) - \frac{m}{m_x}\left(z' - z'(t_r)\right) \tag{25}$$

where $x(t_r) = x_r$, $x'(t_r) = x'_r$, $z(t_r) = z_r$ and $z'(t_r) = z'_r$. The solution for the *y*-motion is simply derived using the transformation equation i.e. $y = x + z$. Hence, the displacement and velocity of the *y*-motion in the case of free-end TMS were derived as Eq. (26) and Eq. (27) respectively.

$$y = \left(1 - \frac{m}{m_x}\right) z + \left[\frac{m}{m_x} z'(t_r) + x'(t_r)\right](t - t_r) + \frac{m}{m_x} z(t_r) + x(t_r) \tag{26}$$

$$y' = \left(1 - \frac{m}{m_x}\right) z' + \frac{m}{m_x} z'(t_r) + x'(t_r) \tag{27}$$

Alternatively, the solution for the free-end TMS can be derived from Eqs. (20-23) but the solution obtained would be the same as when zero initial velocities are assumed. For instance, the solution for the displacement and velocity of the *x*-motion would be $x = x(t_r) - (m/m_x)\left[z - z(t_r)\right]$ and $x' = -(m/m_x)z'$ respectively.

4. Results and Discussions

In this section, the results are discussed in three parts. First, the CPLM solution was verified using published results and

'exact' numerical solutions. Secondly, the application of the closed-form solutions for the *x*- and *y*-motions under special conditions was discussed. Thirdly, the effect of mass ratio on the vibration response of the TMS was examined in details. Also, some theoretical derivations for the limiting mass ratio are presented and discussed.

4.1. Verification of CPLM Solution

In order to verify the CPLM solution, two sets of examples that have been investigated in other studies [3, 4] are re-examined here. The first set of examples is for a TMS with free ends while the second set is for fixed ends. Both sets of examples are based on identical masses in the TMS. The CPLM estimates of natural frequencies are compared with published results [3, 4] and exact results as shown in Tables 1 and 2. The exact results were obtained from numerical solutions derived by integrating the coupled nonlinear ODEs (Eqs. (1) and (2)) using the 'StiffnessSwitching' algorithm in Mathematica™. The 'StiffnessSwitching' algorithm can be used to solve ordinary differential equations numerically and is one of the options available in the NDSolve function of Mathematica™. It is particularly useful for solving difficult (i.e. stiff) nonlinear differential equations and is capable of producing very accurate solutions even when traditional numerical methods (such as Runge-Kutta fourth-order) fail to converge to a solution.

Table 1. Frequency estimates for TMS with free ends

s/n	m_x	m_y	K_{LC}	K_{NLC}	X_0	Y_0	Ref. [3] (% error)	Ref. [4] (% error)	CPLM (% error)	Exact
1	1	1	5	5	5	1	11.1927 (0.00536)	11.4018 (1.874)	11.1972 (0.0456)	11.1921
2	1	1	1	1	10	− 5	18.0316 (0.00776)	18.4255 (2.192)	18.0386 (0.0466)	18.0302
3	5	5	10	10	20	30	17.0685 (0.00762)	17.4356 (2.159)	17.0751 (0.0463)	17.0672
4	10	10	50	− 0.01	− 20	40	2.0799 (0.0192)	2.1448 (3.140)	*2.0843 (0.231)	2.0795
5	1	1	10	5	20	25	14.1521 (0.00495)	14.4049 (1.791)	14.1579 (0.0459)	14.1514
6	100	100	200	300	400	200	415.0871 (0.00822)	424.2688 (2.220)	415.2467 (0.0467)	415.0530

* This result was computed using $n = 100$ while others were computed based on $n = 25$.

Table 2. Frequency estimates for TMS with fixed ends

s/n	m_x	m_y	K_L	K_{LC}	K_{NLC}	X_0	Y_0	Ref. [3] (% error)	Ref. [4] (% error)	CPLM (% error)	Exact
1	1	1	1	1	1	5	1	5.1080 (0.00392)	5.1961 (1.729)	5.1101 (0.0450)	5.1078
2	1	1	1	1	5	5	10	13.5132 (0.00814)	13.8022 (2.147)	13.5184 (0.0466)	13.5121
3	5	5	10	20	30	− 10	10	58.7904 (0.00817)	60.0833 (2.208)	58.8132 (0.0470)	58.7856
4	10	10	50	70	90	20	− 40	215.7290 (0.00821)	220.4972 (2.219)	215.8118 (0.0466)	215.7113
5	10	10	25	20	− 0.05	− 10	10	1.8414 (0.00543)	1.8708 (1.602)	*1.8439 (0.141)	1.8413
6	100	100	200	300	400	− 50	50	239.6652 (0.00822)	244.9653 (2.220)	239.7572 (0.0466)	239.6455

* This result was computed using $n = 100$ while others were computed based on $n = 25$.

The CPLM frequency estimates for the examples in Tables 1 and 2 were obtained for $n = 25$ and have negligible error compared to the exact results. The percentage errors of the CPLM estimates and published results are shown in bracket and were calculate as $100\times|\omega_{ex}-\omega|/\omega_{ex}$ where ω_{ex} is the 'exact' frequency. Note that better CPLM estimates can be obtained by increasing n. For instance, $n = 50$ would give the same order of error as the published results [3].

It was observed that the CPLM frequency estimates for serial number 4 of Table 1 and serial number 5 of Table 2 converged more slowly compared to the other examples. These two examples have negative nonlinear stiffness which represents a soft spring. CPLM simulations (not presented here) for a hard spring with the same magnitude of nonlinear stiffness showed a fast convergence. Additionally, CPLM simulations (not presented here) for soft and hard springs with higher magnitudes of nonlinear stiffness, e.g. when $|K_{NLC}|\geq 1$, revealed that the CPLM solutions for both springs have fast and similar convergence rates. Hence, the slow convergence observed can be attributed to the combined effect of very weak (i.e. $|K_{NLC}|\ll 1$) and soft (i.e. $K_{NLC}<0$) nonlinearity. Due to the relatively slow convergence for the above two examples, more accurate CPLM estimates of the natural frequency were obtained for $n = 100$ as presented in Tables 1 and 2.

Further verification of the CPLM algorithm was conducted by comparing the predicted vibration histories with exact vibration histories obtained from numerical solutions. Sanchez [15] argued that complete validation of a method for finding periodic solutions of nonlinear oscillators must involve verification of the natural frequency and oscillation history. Another study [10] has shown that the error in the displacement history for large-amplitude or strong nonlinear vibrations of Duffing-type oscillators may be within acceptable limits, but the corresponding error in the velocity history may be significant and well beyond acceptable limits. Hence, the CPLM solutions for the displacement and velocity histories were compared with numerical solution as shown in Figs. 4 to 7. In these figures the CPLM plots (solid lines) were obtained using $n = 25$. The CPLM plots match with the exact plots (markers) and this implies that the error in the CPLM solution is negligible.

4.2. Special Conditions in the Vibration of a Two-Mass System

In deriving the periodic solutions of nonlinear oscillators the CPLM algorithm generally requires the use of non-zero initial conditions for each discretization. This inherent feature of the CPLM was transferred to the closed-form solutions for the *x*- and *y*-motions. As a result, the closed-form solutions are based on non-zero initial conditions and different masses too. In this section, the closed-form solutions for some special initial conditions and for identical masses are presented and discussed.

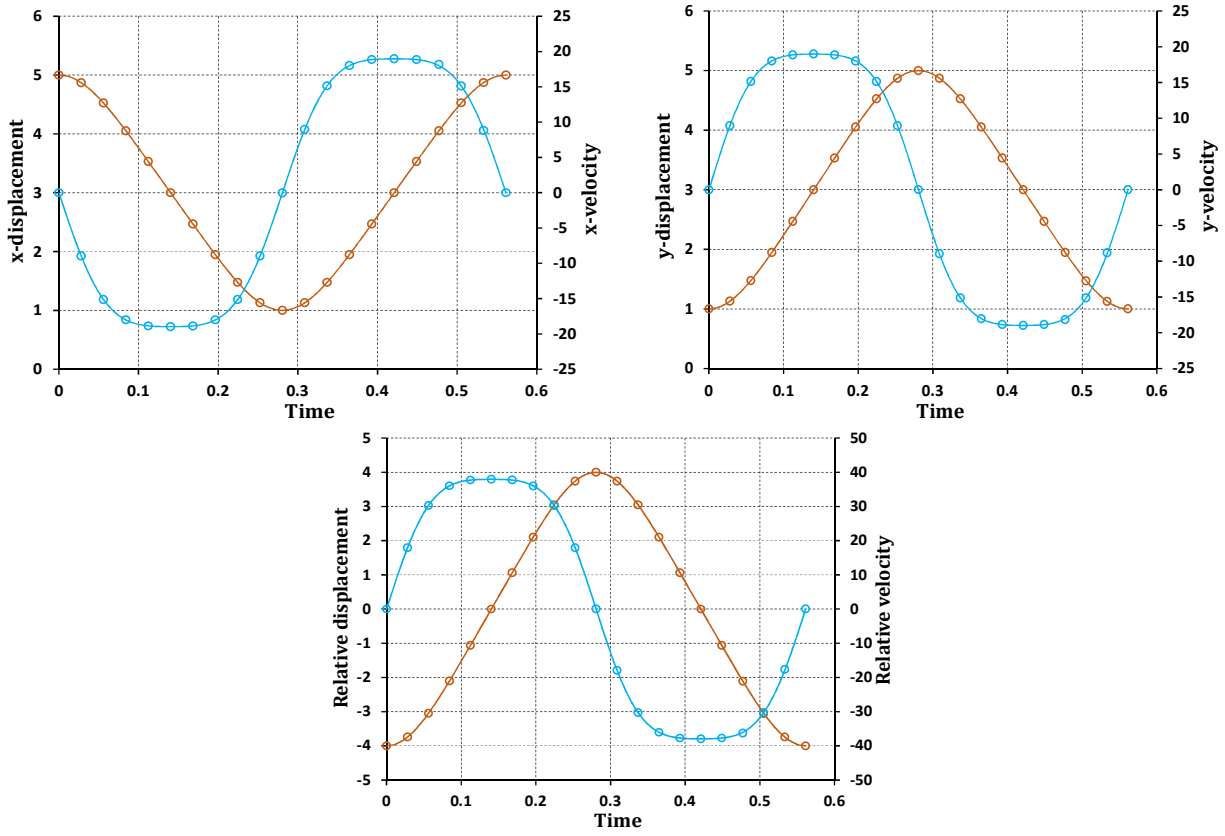

Fig. 4. Displacement (brown) and velocity (blue) histories for a TMS with free ends: $m_x = m_y = 1$; $K_{LC} = 5$; $K_{NLC} = 5$; $x(0) = 5$; $y(0) = 1$; $\dot{x}(0) = \dot{y}(0) = 0$. CPLM – line, exact – marker.

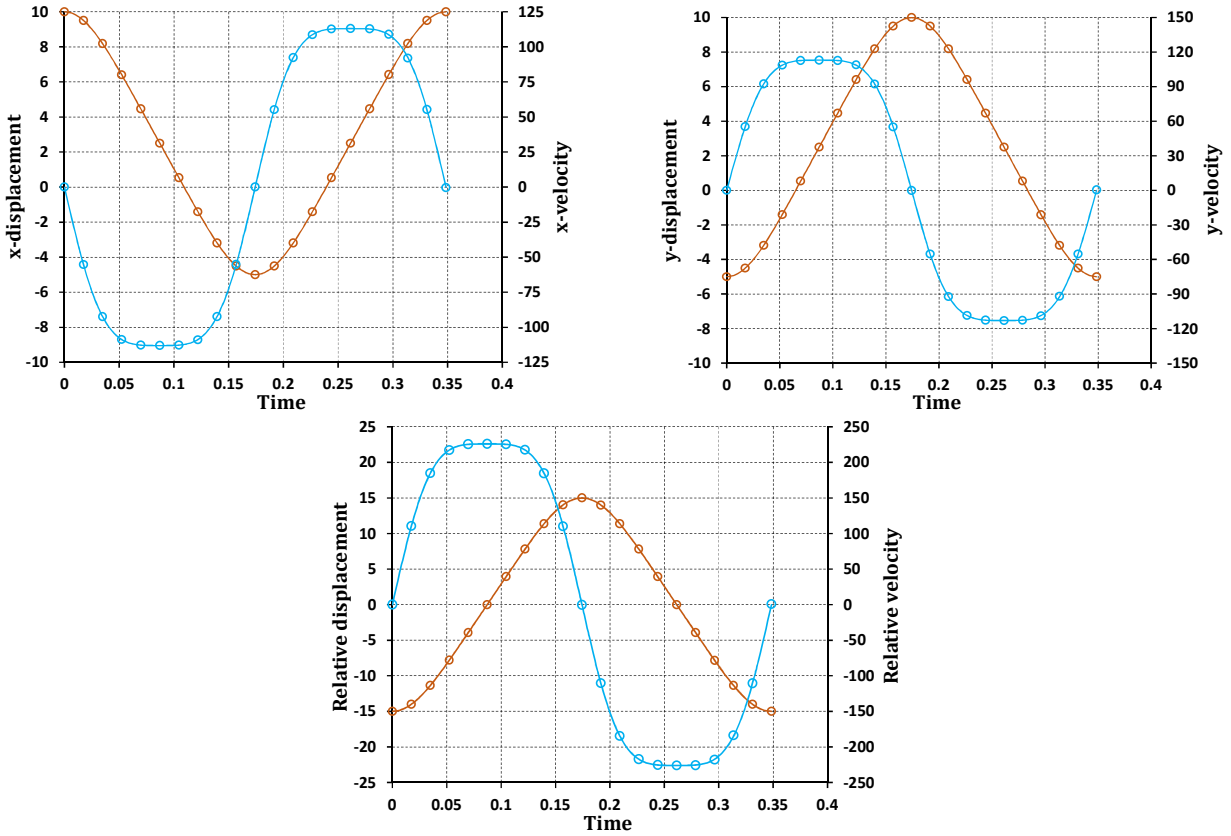

Fig. 5. Displacement (brown) and velocity (blue) histories for a TMS with free ends: $m_x = m_y = 1$; $K_{LC} = 1$; $K_{NLC} = 1$; $x(0) = 10$; $y(0) = -5$; $\dot{x}(0) = \dot{y}(0) = 0$. CPLM – line, exact – marker.

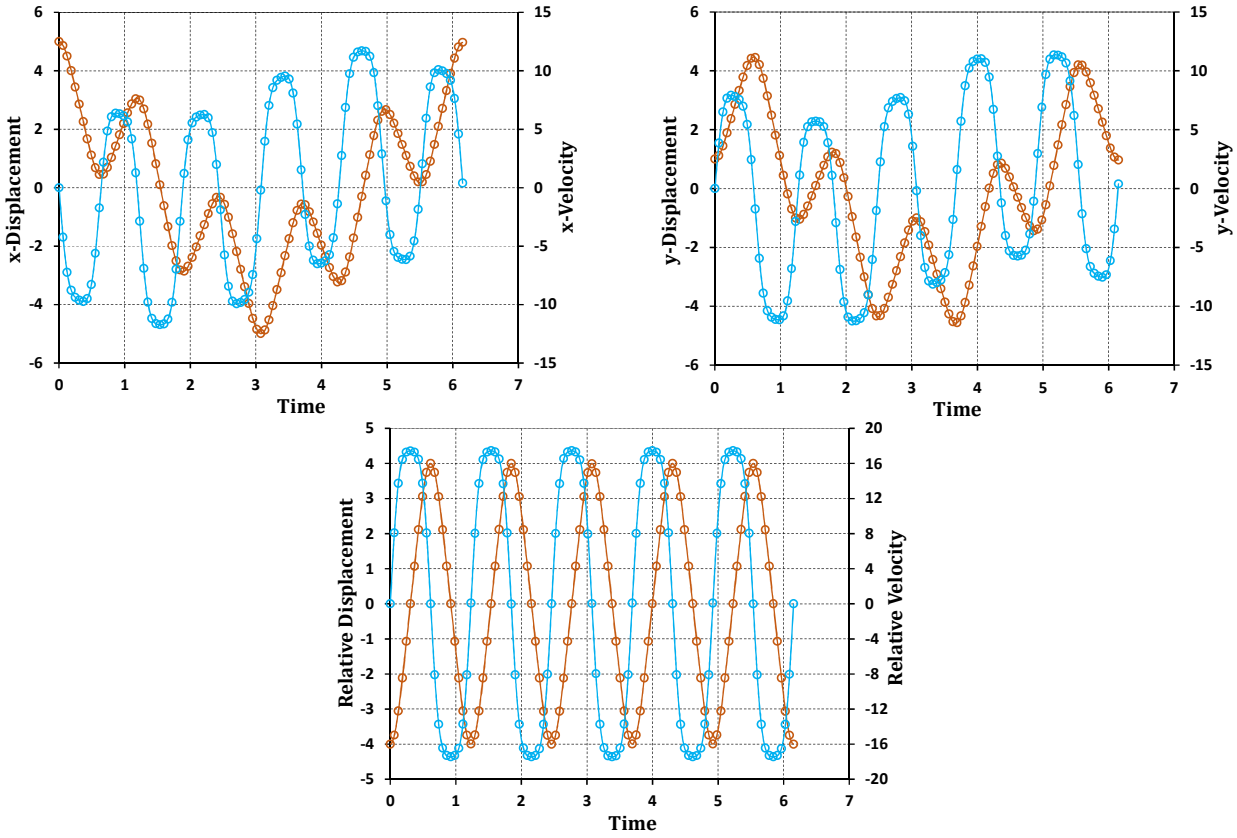

Fig. 6. Displacement (brown) and velocity (blue) histories for a TMS with free ends: $m_x = m_y = 1$; $K_L = 1$; $K_{LC} = 1$; $K_{NLC} = 1$; $x(0) = 5$; $y(0) = 1$; $\dot{x}(0) = \dot{y}(0) = 0$. CPLM – line, exact – marker.

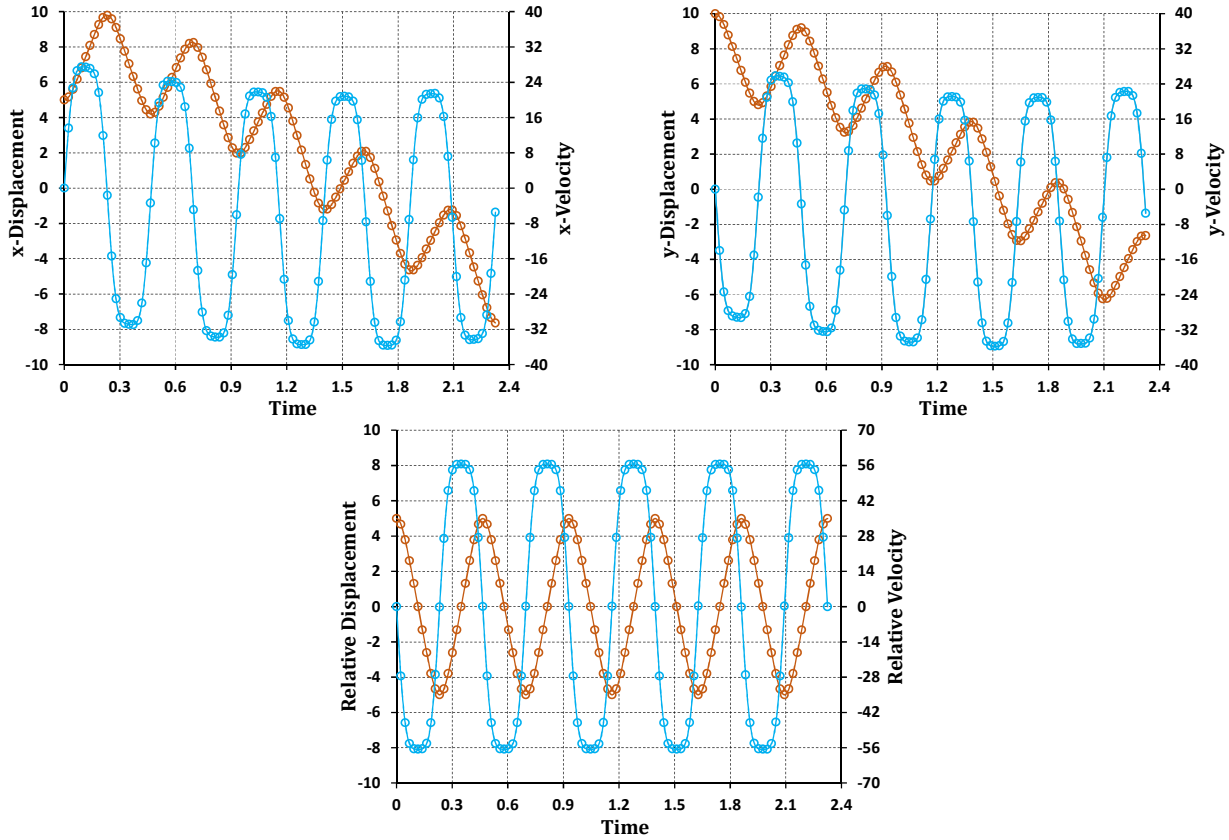

Fig. 7. Displacement (brown) and velocity (blue) histories for a TMS with free ends: $m_x = m_y = 1$; $K_L = 1$; $K_{LC} = 1$; $K_{NLC} = 5$; $x(0) = 5$; $y(0) = 10$; $\dot{x}(0) = \dot{y}(0) = 0$. CPLM – line, exact – marker.

4.2.1. Special Initial Conditions of the Two-Mass System

The special initial conditions normally investigated [1-6] involve non-zero initial displacements and zero initial velocities i.e. $x(0)=X_0$; $y(0)=Y_0$; $x'(0)=0$ and $y'(0)=0$. The corresponding initial conditions for the relative motion of the masses are $z(0)=Y_0-X_0$ and $z'(0)=0$.

(a) Two mass-system with fixed ends

The following conditions hold: $t_r=0$; $x(t_r)=X_0$; $z(t_r)=Y_0-X_0=A$; $x'(t_r)=0$; $z'(t_r)=0$; $x_{Pr}=-(m/m_x)A$ and $x'_{Pr}=0$. These conditions imply that $A_1=0$ and $A_2=X_0+(m/m_x)A$. Hence, from Eqs. (20-23) we get:

$$x=\left[X_0+\left(\frac{m}{m_x}\right)A\right]\cos(\omega_x t)-\left(\frac{m}{m_x}\right)z \tag{28a}$$

$$x'=-\omega_x\left[X_0+\left(\frac{m}{m_x}\right)A\right]\sin(\omega_x t)-\left(\frac{m}{m_x}\right)z' \tag{28b}$$

$$y=\left[X_0+\left(\frac{m}{m_x}\right)A\right]\cos(\omega_x t)+\left(1-\frac{m}{m_x}\right)z \tag{28c}$$

$$y'=-\omega_x\left[X_0+\left(\frac{m}{m_x}\right)A\right]\sin(\omega_x t)+\left(1-\frac{m}{m_x}\right)z' \tag{28d}$$

(b) Two mass-system with free ends

The following conditions hold: $t_r=0$; $x(t_r)=X_0$; $z(t_r)=Y_0-X_0=A$; $x'(t_r)=0$; $z'(t_r)=0$. Hence, from Eqs. (24-27) we get:

$$x=X_0+\frac{m}{m_x}(A-z) \tag{29a}$$

$$x'=-\frac{m}{m_x}z' \tag{29b}$$

$$y=X_0+\frac{m}{m_x}A+\left(1-\frac{m}{m_x}\right)z \tag{29c}$$

$$y'=\left(1-\frac{m}{m_x}\right)z' \tag{29d}$$

4.2.2. Identical Masses in the Two-Mass System

Most of the investigations in the literature are for a TMS with identical masses [1-6]; especially, in the case of fixed-end TMS. For the special case when the masses are identical the following conditions hold in addition to the above stated initial conditions: $m_x=m_y$ and $m/m_x=1/2$.

(a) Two mass-system with fixed ends

$$x=\left(\frac{X_0+Y_0}{2}\right)\cos(\omega_x t)-\frac{1}{2}z \tag{30a}$$

$$x'=-\omega_x\left(\frac{X_0+Y_0}{2}\right)\sin(\omega_x t)-\frac{1}{2}z' \tag{30b}$$

$$y=\left(\frac{X_0+Y_0}{2}\right)\cos(\omega_x t)+\frac{1}{2}z \tag{30c}$$

$$y'=-\omega_x\left(\frac{X_0+Y_0}{2}\right)\sin(\omega_x t)+\frac{1}{2}z' \tag{30d}$$

(b) Two mass-system with free ends

$$x = \left(\frac{X_0 + Y_0}{2}\right) - \frac{1}{2}z \tag{31a}$$

$$x' = -\frac{1}{2}z' \tag{31b}$$

$$y = \left(\frac{X_0 + Y_0}{2}\right) + \frac{1}{2}z \tag{31c}$$

$$y' = \frac{1}{2}z' \tag{31d}$$

These closed-form solutions for the *x*- and *y*-motions (i.e. Eqs. (28) to (31)) remain the same irrespective of the nonlinear stiffness considered.

4.2.3. Numerical Nature of the CPLM Algorithm

The CPLM was formulated as an analytical algorithm but it possesses some qualities of traditional numerical methods and can be implemented as a numerical solution. Similar to the traditional numerical schemes the CPLM algorithm is iterative but in contrast it produces closed-form analytical solutions (see Eqs. 13, 20 to 27) for each iteration. The closed-form solutions can be used to plot the vibration history within the time boundaries of each discretization (i.e. $t_r \le t \le t_s$). Hence, data points for the displacement and velocity of the *z*-motion can be extracted using Eq. (13). The data points of the *z*-motion are numerical solutions which can be substituted directly into the closed-form solutions in Eqs. (20-23) to obtain corresponding numerical solutions for the *x*- and *y*-motions. This numerical approach is particularly useful when the number of discretization used for the CPLM solution is large, say $n \ge 50$, so that $\Delta t = t_s - t_r$ is small. With such large number of discretization, it is not necessary to extract data points within each discretization. Rather the solutions at the end point of each discretization, which are a natural consequence of the CPLM algorithm, provide the necessary data points required for the *z*-motion and are used to obtain numerical solutions for the corresponding *x*- and *y*-motions. This way the CPLM algorithm can be operated as a numerical scheme for the solution of the TMS.

4.3. Effect of Mass Ratio on Vibration Response of the Two-Mass System

4.3.1. Two Mass-System with Free Ends

To investigate the effect of mass ratio on the vibration response of a TMS with free ends the example of serial number 3 in Table 1 is reconsidered. The input values for this example are: $K_{LC} = K_{NLC} = 10$, $X_0 = 20$ and $Y_0 = 30$; also $r_m = m_y / m_x$ where $m_x = 1$ and m_y was varied to get the different mass ratios. For a thorough understanding of the effect of mass ratio on the vibration response of the TMS the displacement, velocity and oscillation frequency were considered. To achieve this, investigations were conducted to determine the influence of mass ratio on (a) the phase response and (b) the oscillation frequency.

(a) Influence of mass ratio on the phase response of two-mass system with free ends

Figure 8 illustrates the phase diagrams for the *x*-, *y*- and *z*-motions for different mass ratios and reveals that the phase diagrams converge to some asymptotic solution as the mass ratio increases. The reason for the convergence is because the mass ratio effect becomes constant as r_m increases thus resulting in the TMS exhibiting an asymptotic (or limiting) response.

Now, if $m_x = 1$ and $m_y >> 1$, then $r_m = m_y / m_x >> 1$ and $m / m_x = (1 + 1/r_m)^{-1} \approx 1$, which implies a constant mass ratio effect. Therefore, the parametric equations for the asymptotic responses of the *x*- and *y*-motions can be derived from Eqs. (31) as: $x = Y_0 - z$, $x' = -z'$, $y = Y_0$ and $y' = 0$. The *z*-motion depends on the effective mass (m) and $m < m_x$ in general, while $m \approx m_x$ under the condition of very large mass ratio. The maximum displacement limit of the *z*-motion is determined by the initial conditions while the maximum velocity limit of the *z*-motion is calculated as: $z' = \pm\sqrt{2\int_A^0 -F(z)dz}$ where $F(z) = K_{LC}z + K_{NLC}z^3$ for the asymptotic condition. Therefore, the asymptotic velocity of the *z*-motion is $z'_\infty = \pm\sqrt{K_{LC}A^2 + (K_{NLC}/2)A^4}$. This means that the phase diagram for the *z*-motion will have a maximum asymptotic velocity of ± 225.83 while the maximum displacement limits are fixed at ± 10, the mass ratio notwithstanding. The maximum asymptotic displacement and velocity of the *z*-motion were substituted into the asymptotic equations for the *x*- and *y*-motions to get the corresponding asymptotic limits as follows: $x_\infty = 30 \pm 10$; $x'_\infty = \pm 225.83$; $y_\infty = 30$ and $y'_\infty = 0$. Consequently, the phase diagram for the asymptotic response of the *x*-motion is elliptical with the above limits and its center is located at point (30, 0). The solution for the asymptotic response of the *y*-motion suggests that the latter converges to a point, (Y_0, 0) = (30, 0). We note that this point does not coincide with the center for the asymptotic response of the *x*-motion because the frames of

reference of the motions differ. Under the asymptotic condition, the mass m_y becomes too heavy and its velocity is negligible. The physical meaning of this asymptotic response is that mass m_y is stationary at the point of its initial displacement while mass m_x exhibits a stable vibration about its center.

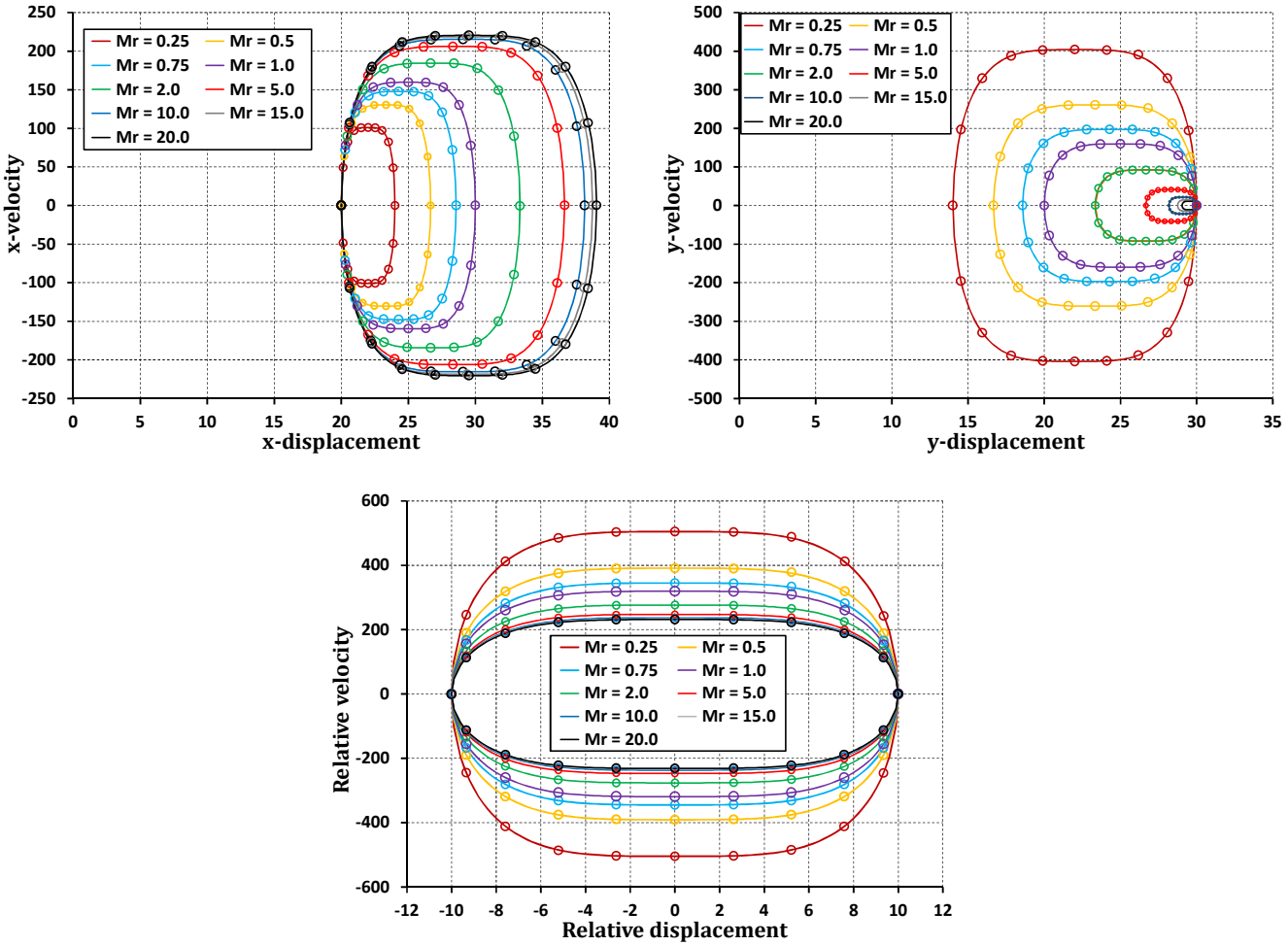

Fig. 8. Effect of mass ratio on phase diagrams for *x*- , *y*- and *z*-motions of a TMS with free ends. CPLM – line, exact – marker.

(b) Influence of mass ratio on the oscillation frequency of two-mass system with free ends

Figure 9 is a plot showing the variation of oscillation frequency with mass ratio for the case study analyzed i.e. serial number 3 of Table 1. There is an initial rapid drop of the oscillation frequency and then a gradual decrease with increasing mass ratio. It was observed that the oscillation frequency approaches a limiting value as the mass ratio becomes very large. An expression to determine this limiting frequency can be derived. First, a normalized time period (T_{nor})was defined as: $T_{nor} = \left(z'_{max} / A\right)T$. For the CPLM, the value of T_{nor} was obtained from the normalized solution. With other approximate analytical techniques [1-6], T_{nor} can be obtained from the frequency-amplitude expression. From the normalized CPLM solution, $T_{nor} = 5.258$. Hence, $T = 5.258\left(A / z'_{max}\right)$ where $z'_{max} = \sqrt{2\int_A^0 -F(z)dz}$ and $F(z) = \left(K_{LC}z + K_{NLC}z^3\right)/m$. Evaluating the expression for z'_{max} gives:

$$z'_{max} = A\sqrt{\frac{2K_{LC} + K_{NLC}A^2}{2m}} \tag{32}$$

which means that the time period can be expressed as a function of mass ratio as shown:

$$T\left(r_m\right) = T_{nor}\sqrt{\frac{2m}{2K_{LC} + K_{NLC}A^2}} \tag{33}$$

where $m = r_m / \left(1 + r_m\right)$ and assuming that $m_x = 1$. As discussed above, if $r_m = m_y / m_x \to \infty$ then $m = m_x$. Therefore,

$$T_{\infty} = T_{nor}\sqrt{\frac{2m_x}{2K_{LC} + K_{NLC}A^2}} \tag{34}$$

On the other hand, if $r_m \to 0$ then the period can be obtained by replacing m_x with m_y in Eq. (34). The limiting frequency is then calculated as $\omega_{\infty} = 2\pi / T_{\infty}$. Applying Eq. (34), the value for the limiting frequency in Fig. 9 was calculated as 26.986.

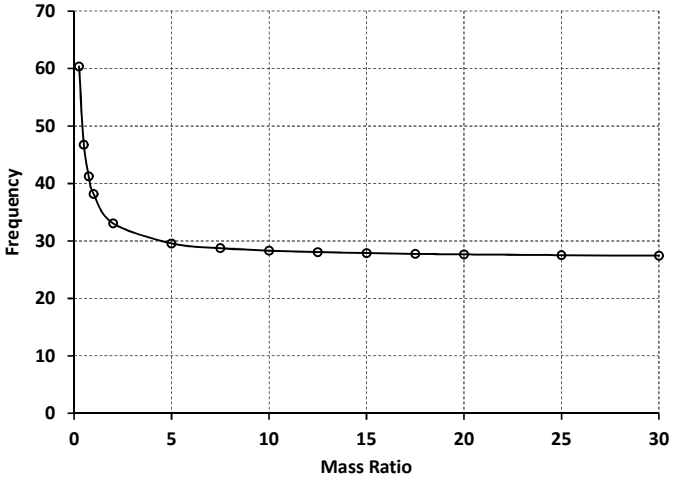

Fig. 9. Variation of nonlinear frequency with mass ratio for a TMS with free ends. CPLM – line, exact – marker.

Additional investigations were conducted to examine the influence of relative amplitude on the frequency-mass ratio relationship. Equation (33) was evaluated at different values of A and a plot of the variation of frequency with mass ratio for various relative amplitudes is shown in Fig. 10. The arrow in the figure shows the direction of increasing relative amplitude. The figure reveals that the oscillation frequency for each mass ratio increases with relative amplitude and that the oscillation frequency for each relative amplitude approaches a limiting value as the mass ratio becomes very large.

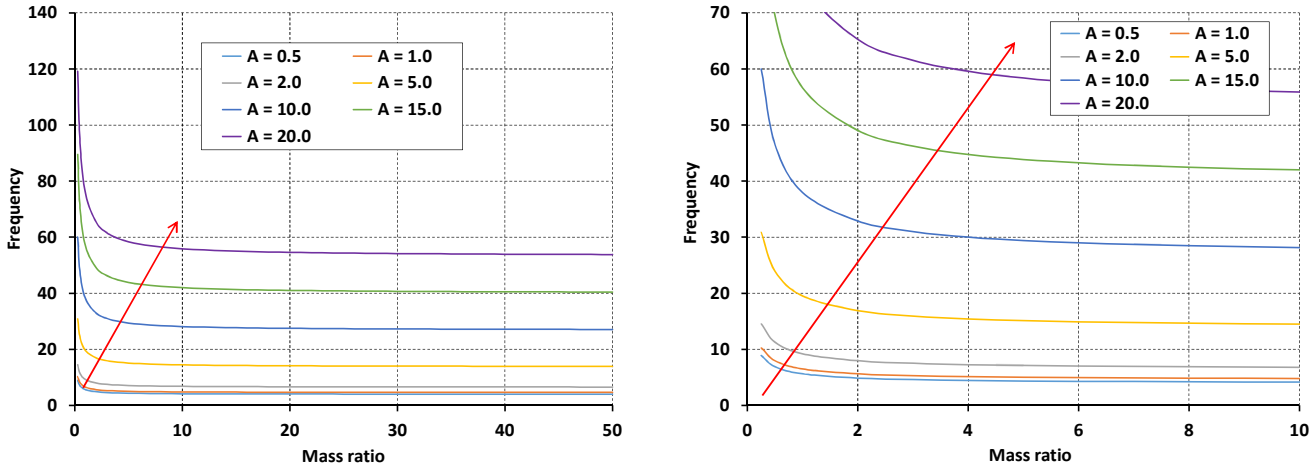

Fig. 10. Variation of nonlinear frequency with mass ratio for different relative amplitudes: left – full, right – amplified.

In the above analysis, the mass m_x was assumed to be equal to one. It will be interesting to see what happens if this restriction is removed. Relaxing such restriction allows for determination of the oscillation frequency where the two masses can assume any value. This can be achieved by redefining the mass ratio as $r_m = m_y / m_x = k\bar{m}_y / k\bar{m}_x$ where $k = m_x$ is a multiplying factor which removes the restriction that $m_x = 1$, $\bar{m}_y = r_m$ and $\bar{m}_x = 1$. The implication is that the frequency-mass ratio relation can be expressed as Eq. (33) with $m = kr_m / (1 + r_m)$ while the limiting time period can be expressed as Eq. (34) where m_x can take any value.

Figure 11 shows the variation of the oscillation frequency for different mass ratios and multiplying factors. The arrow indicates the direction of increasing mass ratio and multiplying factor respectively. It was observed that an increase in the multiplying factor causes a decrease in the oscillation frequency for each mass ratio. An increase in the multiplying factor means that heavier masses are being used even though the mass ratio remains unchanged. Since the oscillation frequency is inversely proportion to the square root of the effective mass (see Eq. (33)) then the oscillation frequency would decrease for the heavier masses as predicted in Fig. 11. The implication of this observation is that the mass ratio alone is not sufficient for understanding the response of the TMS. The individual masses are necessary to get a more complete understanding.

Figure 11 also reveals that limiting responses exist for (a) the frequency-multiplying factor relation as the mass ratio becomes very large and for (b) the frequency-mass ratio relation as the multiplying factor becomes very large. For the frequency-multiplying factor relation the expression for the limiting response can be derived from Eq. (34) as:

$$\omega_{\infty} = \left(\frac{2\pi}{T_{nor}} \sqrt{K_{LC} + \frac{K_{NLC}}{2} A^2} \right) k^{-\frac{1}{2}} \tag{35}$$

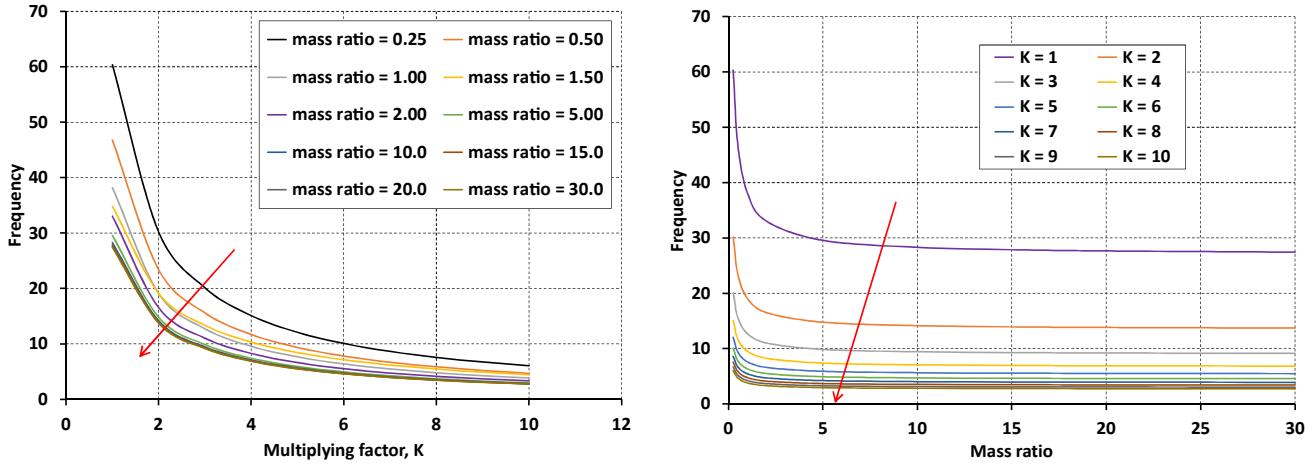

Fig. 11. Variation of nonlinear frequency with (a) multiplying factor for different mass ratios (b) mass ratio for different multiplying factors.

On the other hand, the oscillation frequency decreases with increasing multiplying factor and in the asymptotic limit the frequency is equal to zero. Therefore, the limiting curve for the frequency-mass ratio relation is a horizontal line that coincides with the mass-ratio axis i.e. $\omega_{k\to\infty} = 0$. The physical meaning of this result is that the entire TMS undergoes a rigid body motion for all mass ratios when the masses are very heavy i.e. for very large k-values. The rigid body motion involves translation of the masses by their initial displacements and the coupling spring remains deformed in tension if $z > 0$ or compression if $z < 0$.

4.3.2. Two Mass-System with Fixed Ends

The example of serial number 2 in Table 2 was considered for the TMS with fixed ends. The input values for this example are: $K_L = 1$, $K_{LC} = 1$, $K_{NLC} = 5$, $X_0 = 5$ and $Y_0 = 10$; and the mass ratio is still defined as $r_m = m_y / m_x$ where $m_x = 1$ and m_y is varied to get the different mass ratios.

(a) Influence of mass ratio on the phase response of a two-mass system with fixed ends

The analysis of the effect of mass ratio on the phase diagram for the z-motion is similar to that of Fig. 9. The only difference arises from the restoring force which is now $F(z) = \alpha z + \beta z^3$, where $\alpha = K_L + K_{LC}$ and $\beta = K_{NLC}$ for the asymptotic condition. Thus, the maximum asymptotic velocity can be determined as $z'_{\infty} = \pm\sqrt{\alpha A^2 + (\beta/2) A^4}$. Accordingly, the asymptotic limits for the z-motion were calculated as ± 40.156 and ± 5 for the velocity and displacement respectively. The parametric equations for the asymptotic response of the x- and y-motions can be derived from Eq. (28) as follows:

$$x = Y_0 \cos\left(\sqrt{K_L}\, t\right) - z \tag{36a}$$

$$x' = -Y_0 \sqrt{K_L} \sin\left(\sqrt{K_L}\, t\right) - z' \tag{36b}$$

$$y = Y_0 \cos\left(\sqrt{K_L}\, t\right) \tag{36c}$$

$$y' = -Y_0 \sqrt{K_L} \sin\left(\sqrt{K_L}\, t\right) \tag{36d}$$

The phase diagrams for the x- and y-motions for different mass ratios are shown in Fig. 12. To get a clearer picture of the evolution of the phase diagram the plots were generated for ten oscillation. It was observed that the phase diagrams approach an asymptotic solution as the mass ratio becomes very large.

For the x-motion the phase diagram for each mass ratio is in the form of a coil that tends to stretch out from the origin with increase in the mass ratio as though the coil were in tension. The spiral nature of the asymptotic phase diagram is due to oscillations in the x-motion as predicted in Eqs. (36a) and (36b). Under asymptotic condition (see plot for $r_m = 10^8$ in Fig. 12) the phase diagram for the x-motion has limits of $-15 \le x_{\infty} \le 15$ and $-50.156 \le x'_{\infty} \le 50.156$. On the other hand, the phase

diagram for the *y*-motion is coil-like when the mass ratio is small (i.e. $r_m \le 2$) but under the asymptotic condition it converges to a circle with center at the origin (0, 0) and a radius of 10 (see plot for $r_m = 10^8$). From Eqs. (36c) and (36d) the asymptotic response of the *y*-motion is an ellipse with center at the origin and vertices at ($Y_0\sqrt{K_L}$, 0) and (0, Y_0). In the example considered $K_L = 1$ and this explains why the asymptotic phase diagram for the *y*-motion is a circle.

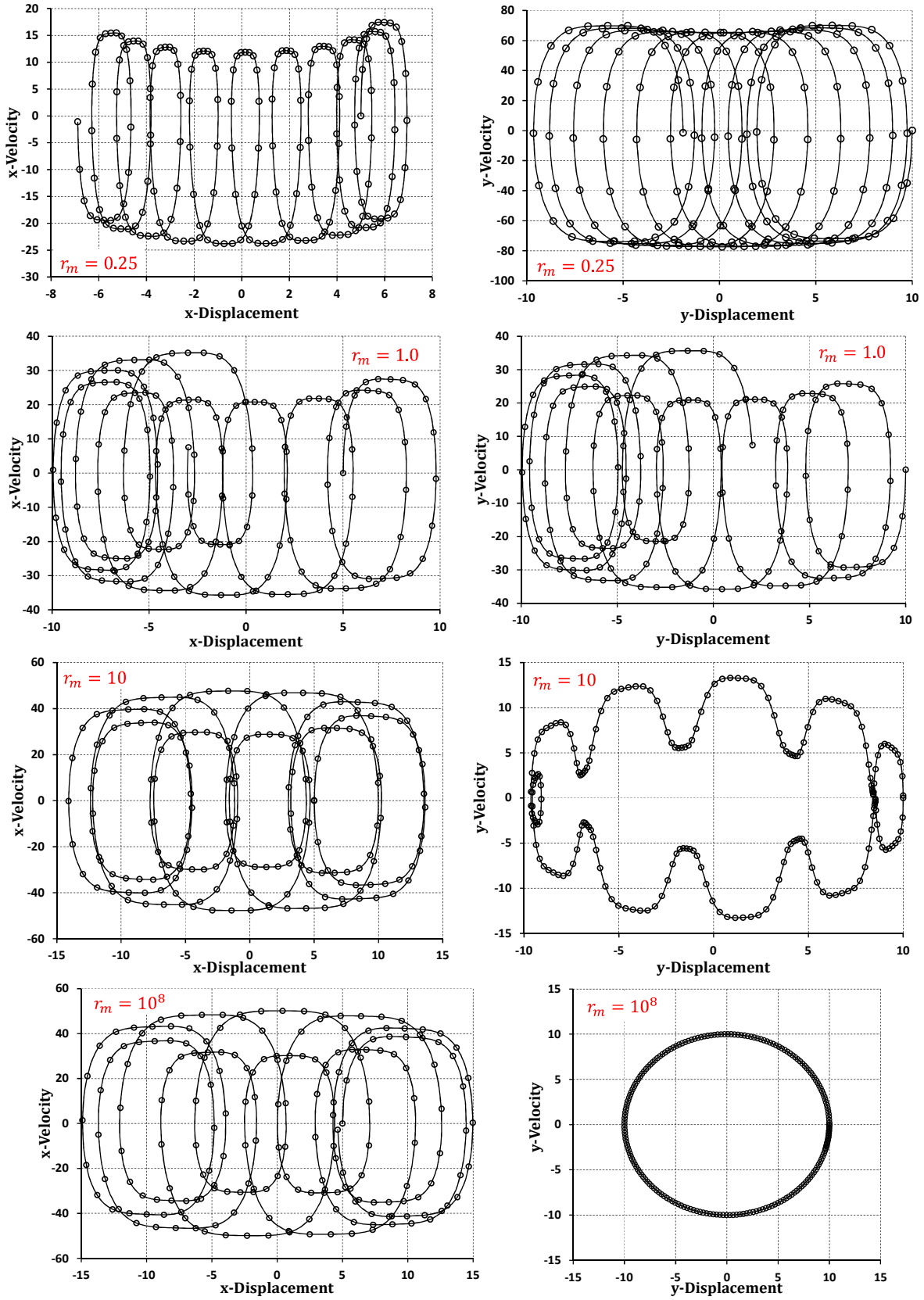

Fig. 12. Effect of mass ratio on phase diagrams for *x*- and *y*-motions of a two-mass system with fixed ends. CPLM – line, exact – marker.

(b) Influence of mass ratio on the oscillation frequency of a two-mass system with fixed ends

The variation of the frequency with mass ratio for a fixed-end TMS is shown in Fig. 13. This figure is similar to Fig. 9 for a TMS with free ends. Following the same analytical approach in section 4.3.1 the limiting frequency was estimated as 9.597.

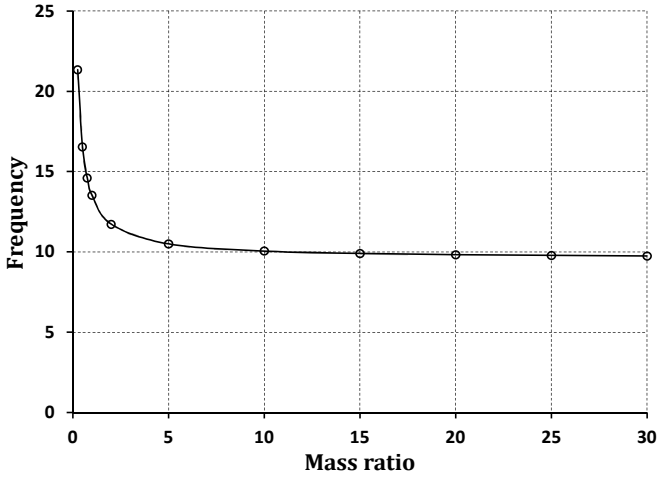

Fig. 13. Variation of nonlinear frequency with mass ratio for a two-mass system with fixed ends. CPLM – line, exact – marker.

Additionally, investigations on the (a) frequency-mass ratio relation for different relative amplitudes and multiplying factors and (b) frequency-multiplying factor relation for different mass ratios were conducted for the TMS with fixed ends and the results obtained are similar to Figs. 10 and 11. Consequently, the analysis and conclusions derived from Figs. 10 and 11 are applicable for the TMS with fixed ends. The reason for the similarity can be attributed to the fact that the oscillation frequency is a function of the relative motion and the relative motion of both the free and fixed end TMS are in the same basic form of a cubic-Duffing oscillator (see Eq. (9)).

4.4. Stability of the Two-Mass System

The stability of the present TMS can be understood by considering the restoring force of the relative motion described by Eq. (9). The restoring force of the present TMS, which is $F(z)=\alpha z+\beta z^3$, can be used to determine the equilibrium points [16, 17] while its derivative, which is $F'(z)=\alpha+3\beta z^2$, determines the nature of the equilibrium points i.e. whether the equilibrium points are stable or not [16, 17]. The equilibrium points are determined by solving the equation $F(z)=0$ which gives $z_1=0$ and $z_{2,3}=\pm\sqrt{-\alpha/\beta}$ for the relative motion. Since the simulations in Figs. 8 and 12 are for positive stiffness constant, the present stability analysis was limited to $K_L>0$, $K_{LC}>0$ and $K_{NLC}>0$. In that case, $z_1=0$ is the only real equilibrium point and this point is stable because $F'(0)=\alpha>0$. This explains the elliptical loops around the origin in the phase diagram of the z-motion shown in Fig. 8. The corresponding equilibrium points for the x- and y-motions of the TMS with free ends are $x_1=y_1=\left[X_0+\left(m/m_x\right)A\right]$ and these equilibrium points are stable as shown in Fig. 8. For the fixed-end TMS, there is no stable equilibrium for the x-motion even under asymptotic condition, while a stable equilibrium exists for the asymptotic y-motion at $y_1=0$ (see Fig. 12). Detailed stability analyses of the present TMS would require consideration of different stiffness conditions and is beyond the scope of the present work, but can be considered in future research endeavors.

5. Conclusion

In this paper, the coupled nonlinear vibrations of a new fixed-end TMS has been investigated analytically. Unlike previous studies, the new fixed-end TMS permits uncouple solutions for non-identical masses and gives a broader leverage for machine design. Simple analytical solutions were derived based on the CPLM and used to perform analysis of the response characteristics of the TMS, especially for different mass ratios. In conclusion, the contributions of the present work are:

1. Development of dynamic models for fixed-end TMS consisting of different masses. Existing studies have been limited to models with identical masses but the present work broadens the scope of the models to account for different masses. The present fixed-end TMS with different masses can be applied in the analysis of coupled systems such as double beam structure and machine components.
2. Application of CPLM for solution of the coupled nonlinear ODEs for the vibration of the fixed-end TMS. The CPLM was applied in an easy and straightforward manner to develop analytical solutions for the response of the TMS. Verification of the CPLM solution by comparing with published results and exact numerical solutions showed that the algorithm is highly accurate and easy to implement compared to other solutions such as Newton harmonic balance method [3].
3. Derivation of closed-form solutions for the vibrations of the masses (i.e. x- and y-motions) through the CPLM algorithm. Exact closed-form solutions were derived for the response of the two-mass system under general initial conditions and where the masses are different. The exact closed-form solutions are independent of the complexity of the nonlinear

restoring force and can be applied with any solution method for solving single-DOF nonlinear oscillators. The exact solutions are considerably simple and give better physical insight compared to previously published solutions of the TMS.

4. Investigation of the effect of mass ratio on the vibration response of a fixed-end TMS. To the best of the authors' knowledge, this paper present the first attempt at investigating the effect of mass ratio on the nonlinear response of a fixed-end TMS. Detailed investigations were conducted that revealed the existence of asymptotic solutions for the vibration of the masses as the mass ratio becomes very large. Hence, analytical expressions for the asymptotic solutions were derived. It was observed that an increase in the mass ratio caused a decrease in the oscillation frequency. Also, it was observed that different mass combinations with the same mass ratio produced different responses. The investigations showed that the mass ratio alone does not give a satisfactory picture of the response of a two-mass system. The individual masses that make-up the mass ratio are also necessary for a more complete understanding.

Acknowledgments

The authors wish to express their gratitude to Mr. Sylvanus Alibi who processed some of the results and assisted in typing some of the equations.

Conflict of Interest

The authors declared no potential conflicts of interest with respect to the research, authorship and publication of this article.

Funding

The authors received no financial support for the research, authorship and publication of this article.

References

[1] Cveticanin, L., Vibrations of a coupled two-degree-of-freedom system, *Journal of Sound and Vibration*, 247(2), 2001, 279-292.
[2] Cveticanin, L., The motion of a two-mass system with non-linear connection, *Journal of Sound and Vibration*, 252(2), 2002, 361-369.
[3] Lai, S.K., Lim, C.W., Nonlinear vibration of a two-mass system with nonlinear stiffnesses, *Nonlinear Dynamics*, 44, 2007, 233-249.
[4] Hashemi Kachapi SHA., Dukkipati, R.V., Hashemi, K.S.Gh., Hashemi, K.S.Mey., Hashemi, K.S.Meh., Hashemi, K.SK., Analysis of the nonlinear vibration of a two-mass-spring system with linear and nonlinear stiffness, *Nonlinear Analysis: Real World Applications*, 11, 2010, 1431-1441.
[5] Bayat, M., Shahidi, M., Barari, A., Ganji D., Analytical Evaluation of the Nonlinear Vibration of Coupled Oscillator Systems, *Z. Naturforsch.,* 66a, 2011, 67-74.
[6] Ganji, S.S., Barari, A., Ganji, D.D., Approximate analysis of two-mass–spring systems and buckling of a column, *Computers and Mathematics with Applications*, 61, 2011, 1088-1095.
[7] Cveticanin, L., KalamiYazdi, M., Saadatnia, Z., Vibration of a two-mass system with non-integer order nonlinear connection, *Mechanics Research Communications*, 43, 2012, 22-28.
[8] Cveticanin, L., Vibrations of a free two-mass system with quadratic non-linearity and a constant excitation force, *Journal of Sound and Vibration*, 270, 2004, 441-449.
[9] Cveticanin, L., A solution procedure based on the Ateb function for a two-degree-of-freedom oscillator, *Journal of Sound and Vibration*, 346, 2015, 298-313.
[10] Big-Alabo, A., Periodic solutions of Duffing-type oscillators using continuous piecewise linearization method, *Mechanical Engineering Research*, 8(1), 2018, 41-52.
[11] Big-Alabo, A., Harrison P., & Cartmell, M.P., Algorithm for the solution of elastoplastic half-space impact. Force-Indentation Linearization Method, *Journal of Mechanical Engineering Sciences*, 229(5), 2015, 850-858.
[12] Big-Alabo, A., Cartmell, M.P., & Harrison P., On the solution of asymptotic impact problems with significant localised indentation, *Journal of Mechanical Engineering Sciences*, 231(5), 2017, 807-822.
[13] Big-Alabo, A., Rigid body motions and local compliance response during impact of two deformable spheres, *Mechanical Engineering Research*, 8(1), 2018, 1-15.
[14] Big-Alabo, A., Equivalent impact system approach for elastoplastic impact analysis of two dissimilar spheres, *International Journal of Impact Engineering*, 113, 2018, 168-179.
[15] Sanchez, N.E., A view to the new perturbation technique valid for large parameters, *Journal of Sound and Vibration*, 282, 2005, 1309-1316.
[16] Nayfeh, A.H. and Mook, D.T., *Nonlinear oscillations*, John Wiley & Sons, New York, 1995.
[17] Jordan, D.W. and Smith, P., *Nonlinear ordinary differential equations: Problems and solutions*, Oxford University Press, Oxford, 2007.